Performance Analysis of Aerocapture Systems for Uranus Orbiters

Rohan G. Deshmukh*, Soumyo Dutta†, Eli Shellabarger*, James B. Scoggins*, Andrew Gomez-Delrio*, Rafael A. Lugo‡
NASA Langley Research Center, Hampton, VA 23681, USA

Pardha Sai Chadalavada§ Joseph D. Williams¶, Justin Garland‖
Analytical Mechanics Associates, Hampton, VA 23666, USA

Breanna J. Johnson*, Daniel A. Matz†, Joshua K. Geiser*
NASA Johnson Space Center, Houston, TX 77058, USA

Jonathan Morgan*
NASA Ames Research Center, Moffett Field, CA 94035, USA

Ricardo Restrepo* and Declan Mages*
Jet Propulsion Laboratory, Pasadena, CA 91109, USA

A Uranus orbiter and probe mission is the highest priority science mission of the current decade. Aerocapture can be employed to support these missions by enabling shorter interplanetary trajectories and requiring less fuel for orbit insertion. This paper investigates the trajectory design and performance analysis of Uranus aerocapture using an MSL-derived aeroshell design. The trajectory tradespace for Uranus aerocapture is investigated to understand the relationship between interplanetary arrival speed and aeroshell aerodynamics to controllability. A 3 degree-of-freedom simulation framework is developed to assess the performance of bank angle fully numerical predictor-corrector aerocapture guidance. A series of Monte Carlo sensitivity studies are conducted to assess the effects that arrival navigation, arrival speeds, and atmosphere knowledge have on the aerocapture robustness and performance. The results suggest that bank angle modulation is a feasible option for Uranus orbit insertion where aerocapture can reduce transit times by 40% and save 1950 kg in propellant mass.

I. Nomenclature

BC	=	Ballistic Coefficient
BAM	=	Bank Angle Modulation
L/D	=	Lift-to-Drag Ratio

II. Introduction

The recently-released National Academies Planetary Science and Astrobiology Decadal Survey 2023-2032 [1] identified the Ice Giants as the top priority science destination for the current decade. While the survey acknowledged the potential for either a Uranus Orbiter and Probe (UOP) mission or a Neptune-Triton Odyssey mission, it ultimately identified the former as the highest priority new flagship mission. The UOP mission calls for a launch window of opportunity between 2031-2038 with a 12-15 year interplanetary cruise time along with a fully-propulsive Uranus

*Aerospace Engineer, AIAA Member.
†Aerospace Engineer, AIAA Associate Fellow.
‡Aerospace Engineer, AIAA Senior Member.
§Aerospace Engineer, Associated with NASA Langley Research Center, AIAA Member.
¶Aerospace Engineer, Associated with NASA Ames Research Center, AIAA Member.
‖Planetary Scientist

Orbit Insertion burn on the order of a few km/s [2, 3]. However, a mission to Uranus with the same science payload could utilize aerocapture for orbit insertion to achieve a significant reduction in both the interplanetary cruise time and propulsive burn costs. Less propulsive burn allows for less propellant mass, which otherwise could be allocated to science payload (e.g. additional probe).

Aerocapture is a promising propellant- and time-saving orbital insertion technique for atmosphere-bearing destinations such as Uranus. Figure 1 provides a visualization of the aerocapture concept of operations for Uranus orbit insertion. The cruise stage approaches Uranus's sphere-of-influence on a hyperbolic trajectory. The cruise stage on-board navigation is used to target the entry interface point, which is defined at 1000 km altitude. Prior to entry, the cruise stage is jettisoned leaving the protective aeroshell encapsulating the orbiter and probe to enter Uranus's atmosphere. The trajectory can be designed based on the vehicle's arrival speed and aerodynamic properties. Active guidance is utilized to steer the aeroshell during atmospheric flight such that the vehicle exits the atmosphere with the targeted apoapsis. Atmospheric flight duration is on the order of minutes. Upon exiting the atmosphere, the heatshield and backshell are jettisoned leaving the orbiter and probe in the post-aerocapture orbit. Upon reaching apoapsis of the post-aerocapture orbit, a periapsis raise maneuver is performed to raise periapsis to the science orbit. If no raise burn is done, the subsequent inbound leg of the orbit would re-enter the atmosphere. Finally, upon reaching periapsis of the orbit, an apoapsis correction burn is performed to correct for any apoapsis targeting errors. The target orbit can be determined to achieve the desired science orbit, such as enabling flybys of the Uranian moon Titania. Despite requiring two propulsive burns for orbit insertion, aerocapture can significantly reduce the cost to the order of meters per second as compared to kilometers per second with fully-propulsive methods.

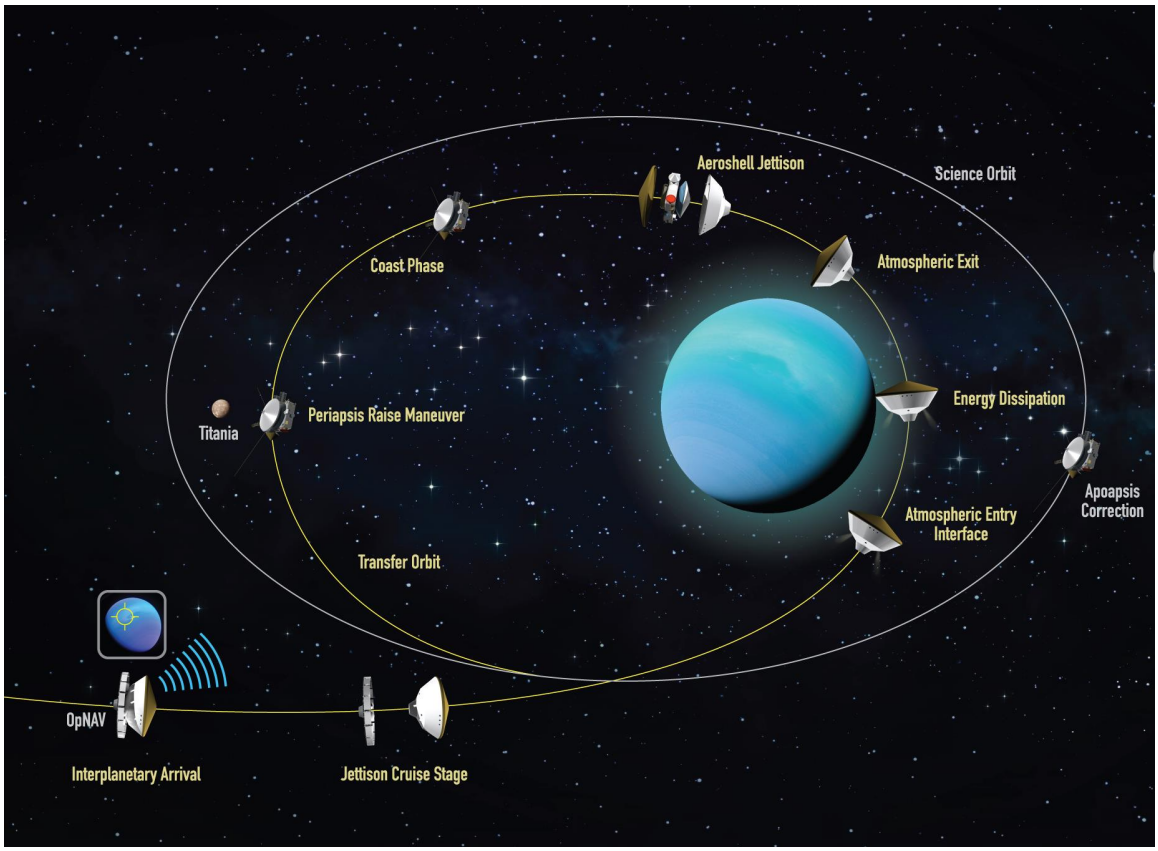

Fig. 1 Aerocapture Concept of Operations

Although not flight-proven, previous aerocapture systems studies have demonstrated both the validity and robustness of the maneuver at various planetary destinations. Of the two Ice Giants, Netpune has been the dominant subject for aerocapture performance analysis. For science missions at Neptune, aerocapture has been shown to be capable of delivering up to 1.4 times more delivered mass to orbit than a fully-propulsive mission for the same launch vehicle while reducing interplanetary cruise times by more than 3 years [4, 5]. Additionally, with modern guidance and control,

Neptune aerocapture with blunt-body aeroshells is realizable [6, 7]. Existing literature investigating Uranus aerocapture is scarce and those studies that do exist tend to provide only a preliminary feasbility analysis [8]. Consequently, the two-year NASA Space Technology Mission Directorate (STMD)-funded project, titled Aerocapture System as an Enabling Technology for Ice Giants Missions, aims to mature the analysis and technology state of Uranus aerocapture. This paper is part of a series of project papers that are presented at 2024 AIAA SciTech. An overview of the project can be found in [9]. Detailed information on the interplanetary trajectory design and navigation solutions can be found in [10]. Information of Uranus aerocapture guidance and control strategies can be found in [11]. Information on Uranus aerocapture aerodatabase development can be found in [12]. Information on the Uranus aerocapture aeroheating environment can be found in [13]. Information of Uranus aerocapture thermal protection system design can be found in [14]. Information on Uranus aerocapture aeroshell design can be found in [15].

This paper presents the current state of the trajectory design in support of the new aerocapture project. Section I presents the investigation of the Uranus aerocapture design-space. Section II presents the numerical simulation architecture and baseline Uranus aerocapture trajectory results. Section III presents Monte Carlo sensitivity studies. Section IV presents future work and conclusions.

III. Uranus Aerocapture Design-Space

An assessment of the Uranus aerocapture design-space is conducted for a range of ballistic coefficients, lift-to-drag ratios, and arrival velocities. The objective is to understand the trends of key aerocapture performance metrics as a function of the parameterized design values. The results provide an understanding of the aerocapture design-space and qualitative metrics on trajectory design considerations.

Figure 2 shows the trends for the key metrics of peak total heat rate, max heat load, peak deceleration, middle entry flight path angle, corridor width, and flight envelope. Description of metrics are provided in paragraph below. Figure 2(a) and Figure 2(b) highlight the aeroheating environment. Increasing L/D and ballistic coefficient serve to increase both peak heat rate and max integrated heat load. These two metrics are commonly used in thermal protection system material selection and thickness sizing. Higher heat rates can lead to need for newer materials while higher lead loads can lead to larger thickness, thereby increasing the thermal protection system mass. The values in Figure 2(a) and Figure 2(b) are within the performance capability range of conformal PICA. Figure 2(c) highlights the aerodynamic loading environment and shows peak deceleration to strongly increase with L/D and remain fairly constant with ballistic coefficient. The loading environment is an important metric for aeroshell structural load consideration. Figure 2(e) shows the corridor width, which is defined by the lift up (steep) and lift down (shallow) trajectories. The width defines the theoretical controllability limits. Figure 3 shows a sample corridor bound trajectory. The midpoint entry flight path angle between these two trajectories is shown by Figure 2(d). Increasing ballistic coefficient and L/D both lead the midpoint entry flight path angle to become more negative (e.g. steeper). However, only L/D significantly influences the corridor width. Given that corridor width is a quantitative metric for aerocapture controllability, any mass changes (e.g. ballistic coefficient) to the aeroshell are not expected to appreciably influence the vehicle control margin during aerocapture. Trajectory dispersion, such as atmospheric, aerodynamic, or delivery state dispersions, will reduce the corridor margin. Figure 2(f) provides a visualization of how $\pm 3\sigma$ aerodynamic and atmosphere dispersions reduce the corridor width. The dispersions are individually applied using one-variable-at-a-time (OVAT) technique, commonly used in EDL flight mechanics analysis to understand performance sensitivities. The reduced corridor width provides a quantitative value for how much entry flight path angle dispersion the parameterized design can tolerate. The remaining difference between the delivery state dispersion and reduced corridor width indicates the available control margin. Zero or negative control margin would qualitatively signify that the vehicle would be unable to target the desired apoapsis altitude. Figure 2(f) provides the flight envelope for a parameterized design with an L/D of 0.25, ballistic coefficient of 145 kg/m^2, and hyperbolic arrival velocity of 13.6 km/s. These values were purposely chosen to be representative of the baseline scenario presented in Section V.A (MSL-derived aeroshell housing UOP payload mass arriving at Uranus on Falcon Heavy interplanetary trajectory). The figure shows atmosphere dispersions being the main source for reduction of the corridor width. Given a reduced corridor width of 0.2877°, the figure suggests a $\pm\ 3\sigma$ entry flight path angle uncertainty no greater than 0.14° is needed to have positive control margin.

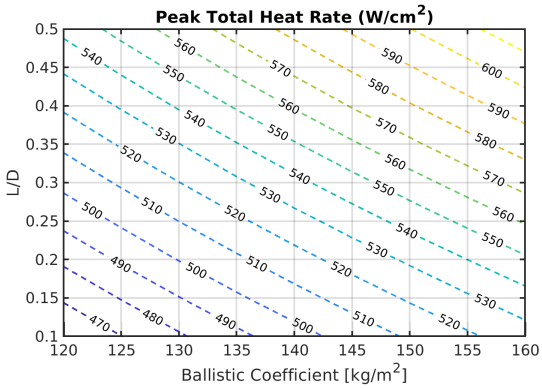

(a) Heat Rate

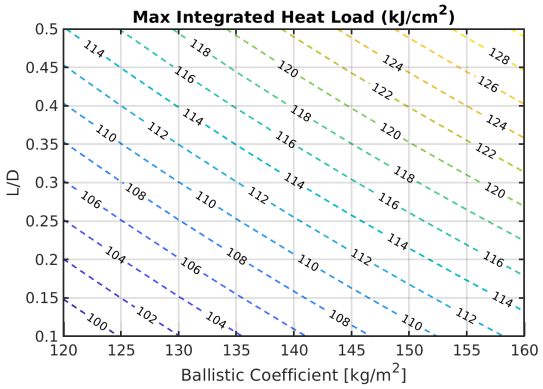

(b) Heat Load

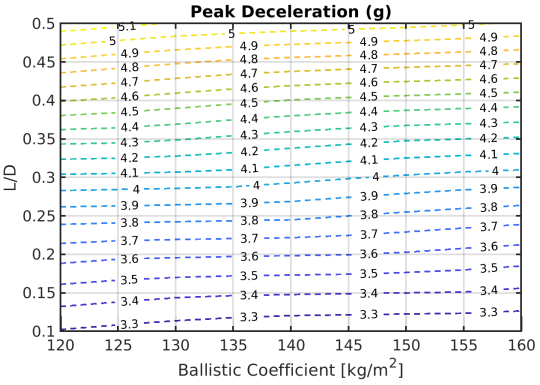

(c) Deceleration

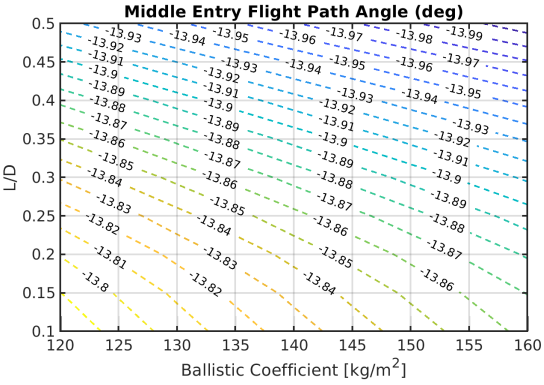

(d) Middle Entry Flight Path Angle

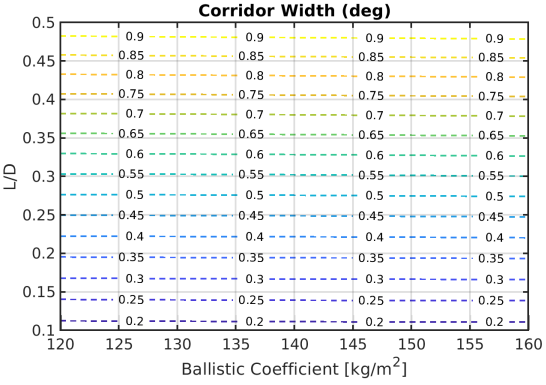

(e) Corridor Width

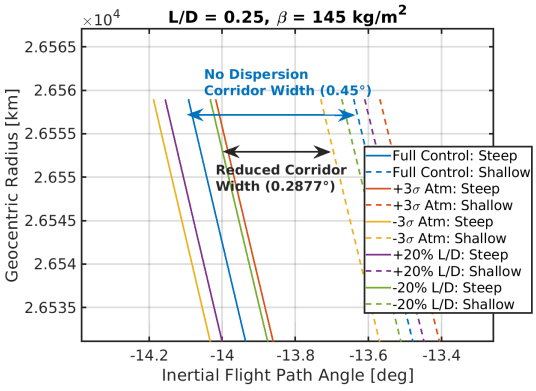

(f) Example Flight Envelope

Fig. 2 Parameterized Uranus Aerocapture Trajectory Trade Space

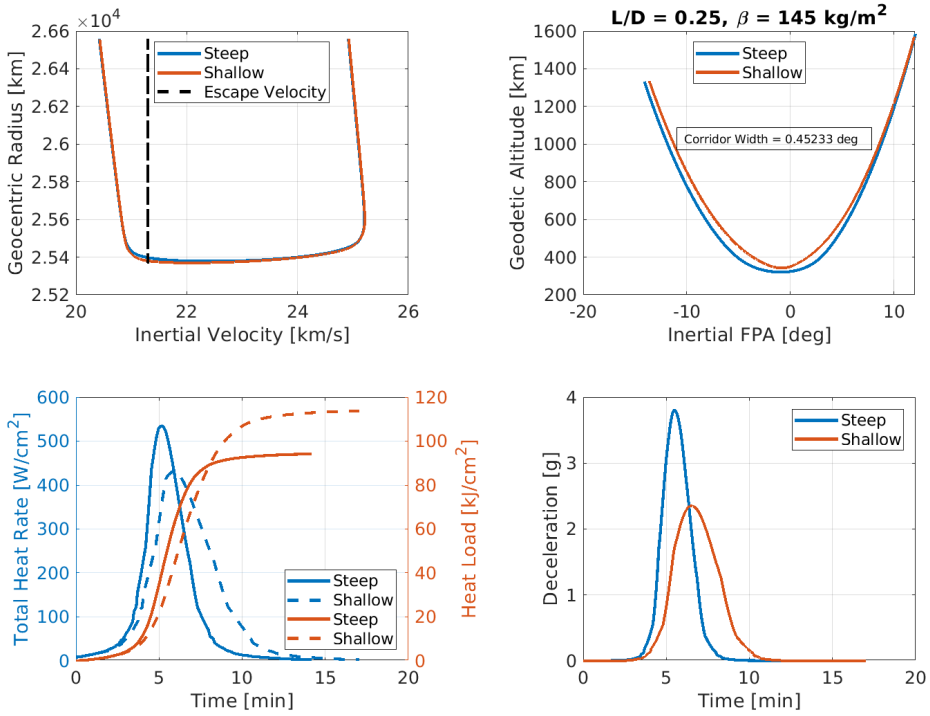

Fig. 3 Sample Corridor Bounding Trajectories

For a Uranus aerocapture mission, one important parameter to consider is the design of the interplanetary trajectory. More information on these trajectories can be found in [10]. The trajectories depend on a variety of factors, including launch year, launch vehicle, and planetary gravity assists. All these factors combined lead to a range in arrival velocities. Nevertheless, the design parameter that is varied in this analysis to capture the general range of these trajectories is the hyperbolic arrival velocity, (V_∞). Figure 4 provide results of the aerocapture trajectory trade-space for a sweep of arrival velocities. Figure 4(a) shows the aeroheating environment increasing exponentially with increasing arrival velocities. Thermal protection system material performance may limit the upper bound of arrival velocities. Figure 4(b) shows the corridor width and reduced corridor width increasing lineally with arrival velocity. Comparing the current delivery state uncertainty width to the reduced corridor width trends can allow for a lower-bound of arrival velocities to be ascertained.

The key takeaways from the investigation of the Uranus aerocapture design-space can be summarized as follows. Reducing ballistic coefficient can serve to reduce the aeroheating environment without affecting the control authority. Increasing L/D and arrival velocity provides a trade-off of more control authority at the expense of increased heating and deceleration concerns. For the baseline design investigated in this paper, the flight envelope indicates positive control margin. Navigation uncertainty greater than $\pm 0.14^\circ$ (3σ) may lead to uncaptured trajectories. The latter finding will be important when understanding the results produced in Section V.B.

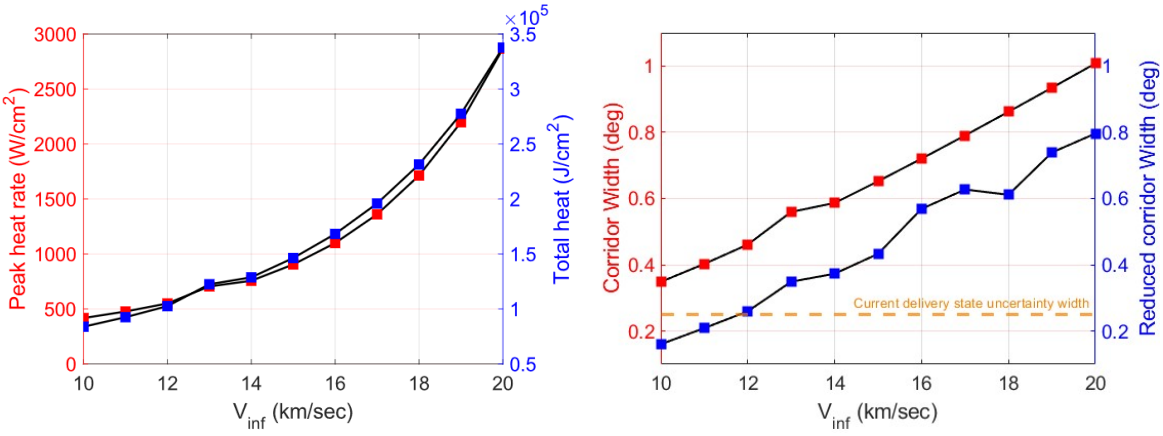

(a) Aeroheating Environment

(b) Corridor Width

Fig. 4 Interplanetary Trajectory Uranus Aerocapture Trajectory Trade Space

IV. Trajectory Simulation Framework

Section III provides an insight into the design-space for Uranus aerocapture trajectories. Candidate designs are selected for end-to-end numerical simulation. This section introduces the trajectory simulation framework developed for assessing Uranus aerocapture performance.

The Program to Optimize Simulated Trajectories II (POST2) [16] is utilized to run Monte Carlo simulations of Uranus aerocapture trajectories. Figure 5 provides a visualization of the simulation architecture and its various subsystems integrated into it. Table 1 provides an overview of the simulation setting utilized. The simulation settings provide the ground-rules for the aerocapture scenario assessed, including target orbit and Monte Carlo inputs. Uranus gravity is modeled using an oblate rotating ellipsoidal gravity model. Uranus Global Reference Atmosphere Model (UranusGRAM) 2021 is utilized as the atmospheric model [17]. UranusGRAM is developed based on Voyager observations to provide atmosphere data that can vary with time, latitude, and longitude. Furthermore, it provides the capability to simulate density dispersions. At the current time, UranusGRAM does not provide atmospheric wind data. Mass properties provide aeroshell definition, including inertia tensor, mass, and center-of-gravity location. A Mars Science Laboratory (MSL)-derived 70° 5m diameter, 1.25m nose radius sphere-cone aeroshell that houses the UOP payload mass is assumed. A maximum possible value mass of 4064.25 kg is utilized in this paper. More technical information on the aeroshell design and mass properties can be found in Reference [15].

The Fully Numerical Predictor-Corrector Aerocapture Guidance (FNPAG) algorithm [18] employing bank-angle modulation is integrated into the POST2 simulation. Perfect onboard state knowledge is assumed. More information on

the FNPAG algorithm development, testing and tuning can be found in Reference [10]. Figure 6 provides a visualization of the Uranus aerocapture guidance, navigation, and control (GNC). Every guidance call at 2Hz, FNPAG solves for the bank angle that minimizes the apoapsis error at exit. The solution is bounded between upper and lower bank angle limits of 15° and 165°, respectively (note: ±15° margin on theoretical max/min bank angle is added). The solution is then passed through a pseudo-control actuator (emulate 6DOF control response in a 3DOF environment) that limits the bank command based on a maximum rate and acceleration.

The SPICE toolkit is utilized for providing Uranus orientation and inertial frame definition at the arrival trajectory epoch. This software is used to convert initial states provided by the interplanetary navigation solution in Earth-Mean-Equatorial J2000 to the body-fixed IAU Uranus inertial frame. Entry state files that model arrival navigation performance are utilized to provide initial position and velocity information. More information on the interplanetary navigation solution can be found in Reference [10].

A Uranus-developed aerodatabase, originally derived from MSL, is utilized to provide vehicle aerodynamics over a wide range of hypersonic flow regimes. The database is populated with computational fluid dynamics (CFD) runs using corridor bounding trajectories found in Figure 3. The corridor trajectories are discretized to provide points to initialize flow conditions in CFD runs. An aerothermodynamics database is utilized to provide high-fidelity estimation of the aeroheating environment during atmospheric flight. Similar to the aerodatabase development, the aerothermodynamics database is developed running CFD cases on corridor bounding trajectories. To provide a wide range of potential aeroheating conditions, the corridor bounding trajectories produced in the V_∞ sweep in Figure 4 are utilized. More information on the aerodatabase can be found in Reference [12] and more information on the aerothermodynamics database can be found in Reference [13].

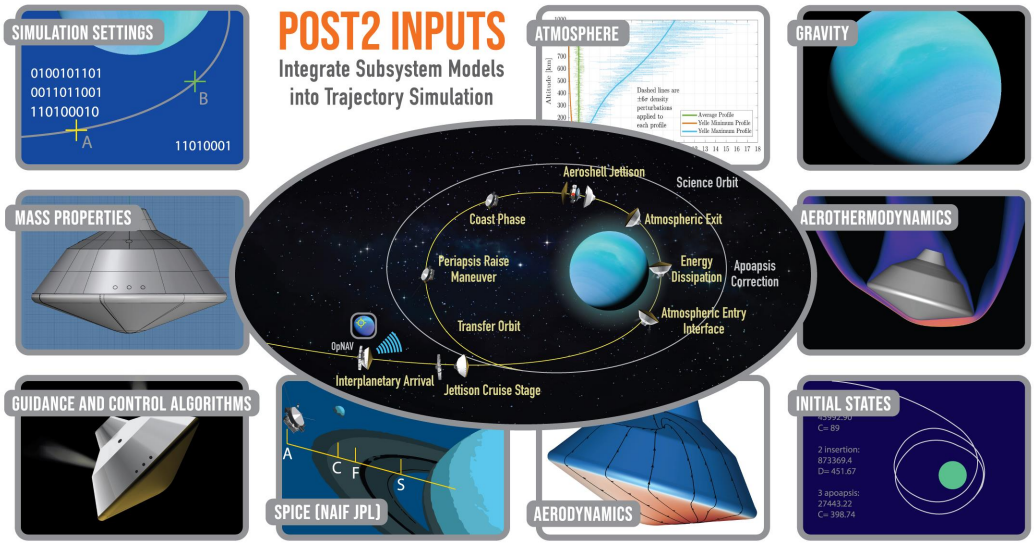

Fig. 5 POST2 Simulation Architecture

Table 1 Simulation Settings for Uranus Aerocapture Trajectories

Category	Variable	Value	Units
Gravity	Equatorial Radius	25559	km
	Polar Radius	24973	km
	J2	0.003343	
	Rotational Rate	-1.012371E-4	rad/s
	Gravitational Constant	5.793951E6	km^3/s^2
SPICE	Binary Files	de430, ura111	
	Leap Second Kernel	naif0012	
	Planetary Constant Kernel	pck00010	
Atmosphere	Atmosphere Entry/Exit Altitude	4000	km
	Guidance Entry/Exit Altitude	1000	km
	Model	UranusGRAM 2021	
Aerodynamics	Hypersonic L/D	0.25	
	Hypersonic Ballistic Coefficient	140	kg/m^3
	Hypersonic Trim Angle of Attack	-17	deg
GNC	Guidance Algorithm	FNPAG	
	Guidance Trigger	0.1	G's
	Guidance Rate	2	Hz
	Onboard Navigation	Perfect State Knowledge	
	Control Method	Bank Angle	
	Control Rate Limit	15	deg/s
	Control Acceleration Limit	5	deg/s
Aerothermal*	Sutton-Graves Constant	8.645E-5	kg^0.5/m
Aeroshell	Mass	4064.25	kg
	Diameter	5	m
	Nose Radius	1.25	m

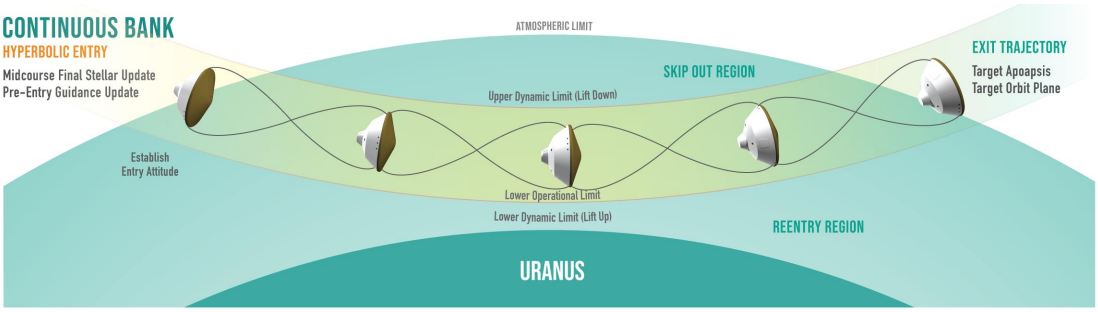

Fig. 6 Visualization of Bank Angle Modulation during Uranus Aerocapture

V. Monte Carlo Analysis

System dispersions such as entry state errors, atmospheric density variations, and, mass properties, aerodynamic coefficient errors are applied using Monte Carlo simulations to assess system robustness. The objective of this analysis is to understand how robust the current aerocapture vehicle design is as well as its sensitivities to the aforementioned

dispersions.

A series of aerocapture performance metrics are developed to quantify the results. Orbit insertion performance is tracked using the post-exit periapsis and apoapsis altitudes along with their corresponding Hohmann transfer ΔV costs. Total ΔV is reported as the sum of the periapsis raise and apoapsis correction burns. Due to the unique out-of-plane alignment of Uranus equator to the ecliptic plane, out-of-plane costs are neglected. It is assumed a post-aerocapture equatorialization, similar to the methodology developed for UOP, will be utilized to provide the out-of-plane change needed (see Reference [10] for more discussion on this topic). Capture success rate is also tracked using the post-exist trajectory characteristics. Trajectories reaching exit with eccentricities greater than or equal to 1 are deemed as uncaptured (parabolic/hyperbolic). Trajectories that do not reach exit are deemed as failed cases. Fortunately, no failed cases exist in the simulations run. Peak deceleration, peak heat rate, and max integrated heat load are reported to provide insight into the environment experienced during aerocapture.

A series of Monte Carlo scenarios are developed and presented in this section. Section V.A presents the baseline scenario, which is subsequently used as the control for the sensitivity scenarios. Section V.B presents the interplanetary navigation sensitivity scenario. Section V.C presents the arrival trajectory sensitivity scenario. Section V.D presents the atmosphere sensitivity scenario.

A. Baseline Scenario

The baseline scenario analyzes aerocapture of a Falcon Heavy interplanetary trajectory with a hyperbolic arrival V_∞ of 13.6 km/s targeting a post-aerocapture orbit of 4000 km x 550000 km. This trajectory has an interplanetary transit time of 8 years with a required ΔV for orbit insertion of 4.5 km/s. As a point of comparison, the UOP study utilized a similarly designed Falcon Heavy interplanetary trajectory but arriving in 13.3 years with a required ΔV for orbit insertion of 1.1 km/s. To achieve the 1.1 km/s Uranus Orbit Insertion (UOI) burn, the UOP study requires 55% of its wet mass to be allocated to propellant. If the UOP study were to conduct UOI with the baseline interplanetary trajectory as aerocapture, then 90% of its wet mass would need to be allocated to propellant. Nevertheless, aerocapture provides the required 4.5 km/s change in ΔV through a single atmosphere pass. This enables the faster arriving interplanetary trajectory cutting Earth to Uranus transit time by 40%.

For the baseline scenario, simulation setting introduced in Table 1 are utilized. The Monte Carlo dispersion settings utilized are shown in Table 2. 8000 Monte Carlo cases are run. The ESF provides dispersed initial states for each Monte Carlo case at E-10 min from navigation covariance analysis. The spherical coordinates of the nominal entry state are provided. UranusGRAM is utilized to disperse the density profile for each Monte Carlo case using a unique random seed. The variable *rpscale* controls the random perturbation scale on the density. A value of 1 produces $\pm 3\sigma$ perturbations. The aerodynamic dispersions are generated internally within the aerodatabase using adders and multipliers on the nominal axial, normal, and side forces. The current setup of the aerodatabase utilizes nominal data generated through Uranus-CFD runs but assumes adder and multiplier dispersion values from MSL aerodatabase. A mass multiplier of $\pm 10\%$ is assumed to assess mass dispersions.

Figure 7 shows the baseline scenario aerocapture orbit insertion performance. Figure 7(a) shows the post-aerocapture apoapsis altitude and periapsis for each Monte Carlo case along with the target apoapsis altitude of 550000 km. Majority of the Monte Carlo cases are scattered around the apoapsis target with only a few outliar cases that significantly overshoot the apoapsis target. Figure 7(b) provides a scatter plot of the apoapsis targeting error vs entry flight path angle (EFPA) for each of Monte Carlo cases mapped to their corresponding total ΔV cost. This plot illustrates the high correction needed for these few outliar cases.

Table 2 Baseline Scenario Monte Carlo Dispersion Settings

Category	Variable	Nominal	$\pm 3\sigma$
Delivery State	Inertial Entry Flight Path Angle	-11.107 deg	From ESF
	Inertial Entry Velocity	24.936 km/s	From ESF
	Entry Altitude	1000 km	From ESF
	Entry Latitude	-9.764 deg	From ESF
	Entry Longitude	190.045 deg	From ESF
	Inertial Entry Azimuth Angle	139.439 deg	From ESF
	Entry - 10 min Epoch	2041-05-20 09:03:08 ET	Fixed
Atmosphere	Random Seed	1	29999
	rpscale	1	
Aerodynamics	Axial Force Adder/Multiplier	0	1
	Normal Force Adder/Multipler	0	1
	Side Force Adder/Multiplier	0	1
Aeroshell	Mass Multiplier	1	0.1

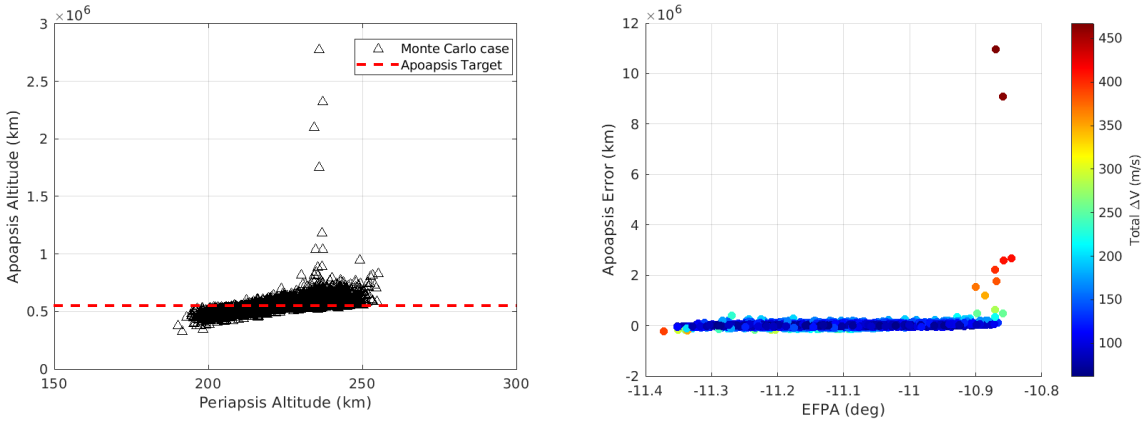

(a) Guidance Apoapsis Targeting Performance

(b) Correlation to ΔV cost

Fig. 7 Baseline Scenario Aerocapture Performance

Figure 8 provides a histogram of the total ΔV cost along with corresponding statistics. Few outliar cases skew the tails of the distribution leading to a 99.87 percentile value of 302 m/s. However, Figure 7(b) provides better context to the aerocapture performance in that majority of the 8000 Monte Carlo cases are indeed low ΔV solutions.

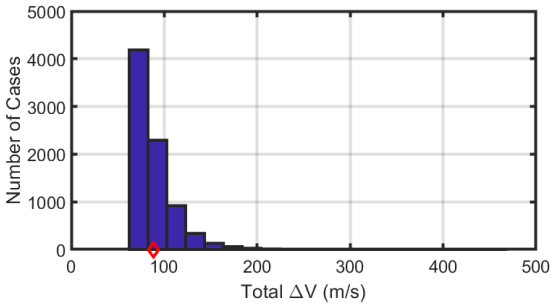

Statistics for Total ΔV (m/s):

Capture Success	=	99.9
Nominal	=	71.0669
Mean	=	88.0269
1-Sigma	=	25.8892
3-Sigma	=	77.6676
0.13 %-tile	=	62.5355
1.00 %-tile	=	62.9181
50.00 %-tile	=	81.4132
99.00 %-tile	=	174.7263
99.87 %-tile	=	301.9475
Minimum	=	62.2836
Maximum	=	467.6477

Fig. 8 Total ΔV Cost for Baseline Scenario

The total ΔV can be utilized with the ideal rocket equation to get an estimate of the required post-aerocapture propellant mass. Assuming a hydrazine propulsion system with an Isp of 200 sec and a ΔV of 302 m/s (99.87 percentile), the resulting propellant mass allocation is 250 kg. As a point of comparison, the UOP allocated 2200 kg to propellant mass allocation for Uranus Orbit Insertion burn. Aerocapture, delivering the same orbiter and probe mass, can reduce the propellant mass allocation needed for orbit insertion by 88%.

Figure 8 also indicates that the capture success rate is 99.9%. The 0.1% of uncaptured cases are hyperbolic with none being failed cases. Figure 9 provides a plot to better understand the reasoning for these remaining hyperbolic cases. Figure 9(a) provide a scatter plot corellation between dispersed hypersonic L/D (from the aerodatabase) and EFPA (from ESF) to captured and hyperbolic cases. The plot indicates no significant correlation to L/D but a correlation of hyperbolic cases to shallower EFPA values. Figure 9(b) explores this correlation even further mapping the post-aerocapture trajectory orbital energy and eccentricity to EFPA. As expected, captured elliptical cases produce negative orbital energy and eccentricity less than 1 and hyperbolic cases produce positive orbital energy and eccentricity greater than 1. With the EFPA for each particular case mapped, the shallower EFPA correlation to hyperbolic cases can be clearly seen. In fact, the general trend shows shallower EFPA lead to more eccentric/larger orbit energy post-aerocapture trajectories. This suggests that the hyperbolic cases could be resolved if the nominal EFPA is biased steeper. This biasing is explored in Reference [11] as a side study but was not incorporated into the analysis presented in this paper. Future work by the ECI project will include this biasing to further tune aerocapture performance. Nevertheless, the preliminary results produced with FNPAG for Uranus aerocapture with this baseline scenario do show promise.

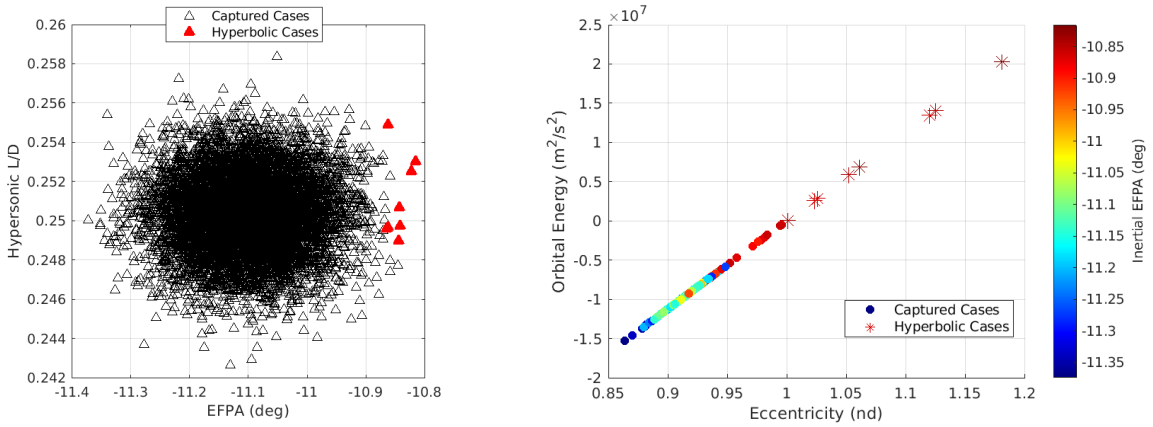

(a) Capture Success Correlation to L/D and EFPA

(b) Post-Aerocapture Orbit Correlation to EFPA

Fig. 9 Understanding correlation between hyperbolic cases and dispersed Monte Carlo inputs

B. Navigation Sensitivity

This section introduces Monte Carlo results assessing the impact of navigation on aerocapture performance.

Interplanetary navigation is a critical component for aerocapture success. The navigation solution defines the uncertainty in the delivered entry interface state. For a Uranus mission, having precise delivery reduces aerocapture uncertainty, increases control margin, and enables full capture success for a wider range of trajectories. The sensitivity of aerocapture performance is assessed based on different navigation solutions. The baseline scenario is used as the control for the comparison. Two burn error scenarios at last trajectory correction maneuvers prior to entry are considered: 0.1x , and 10x burn error. Three navigation scenarios are considered: aggressive ground-in-the-loop, conservative ground-in-the-loop, and fully autonomous. In total, 6 scenarios are analyzed.

Figure 10 shows histograms of the entry interface state for each of the six scenarios. Each navigation solution is mapped to the same entry epoch time and centered at the same nominal entry flight path angle. There is a minute variation to altitude but noticeable variations to longitude, declination, velocity, flight path angle, and azimuth angle. In particular, the 10x burn error and conservative scenarios produce the largest variations. Table 3 shows the 3σ uncertainty values for each scenario.

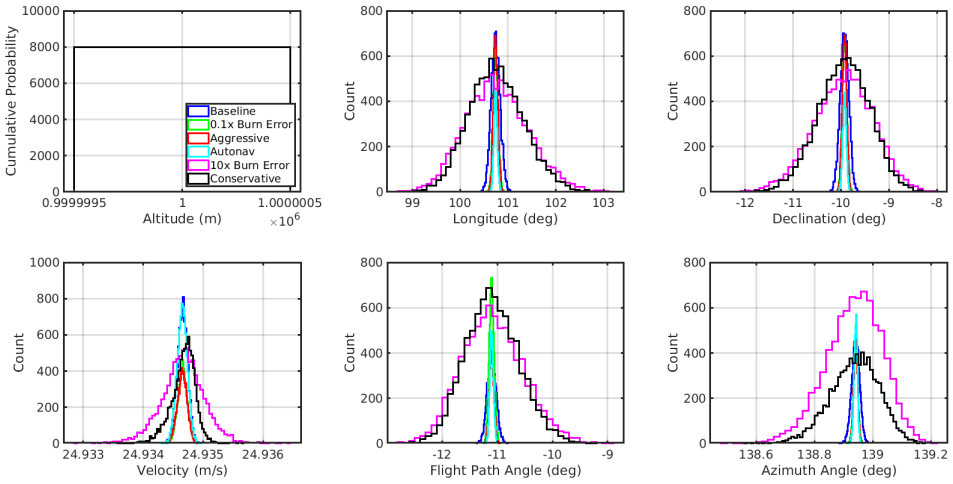

Fig. 10 Uranus Aerocapture Navigation Scenarios at Entry Interface

Figure 11 shows the aerocapture performance comparison between the baseline and the three improved navigation

Table 3 Navigation Solution EFPA

	3σ
Baseline	0.239
0.1x Burn Error	0.130
Aggressive	0.121
Autonav	0.098
10x Burn Error	1.002
Conservative	0.936

scenarios. Reducing the entry flight path angle uncertainty serves to improve the orbit insertion performance. Despite AutoNav providing the most improvement, the new navigation technology is not necessarily needed for Uranus as existing navigation methods, such as reducing TCM burns and aggressive ground-in-the-loop operations, can serve to produce similar improvement.

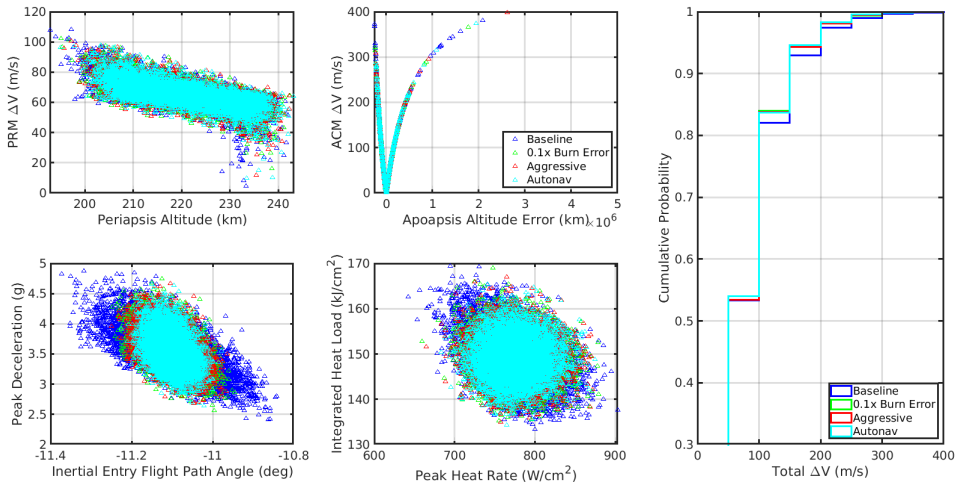

Fig. 11 Uranus Aerocapture performance for Improved Navigation Scenarios

Figure 12 shows the aerocapture performance comparison between the baseline and the two degraded navigation scenarios. Both of these scenarios, with large entry flight path angle uncertainties, serve to stress the aerocapture success rate and orbit insertion performance. On the steep-side, the trajectories dissipate too much energy to the point of exiting the atmosphere with high peak heat rates and negative periapsis altitudes and apoapsis errors (e.g. undershooting the target). All these trajectories still remain captured into a low period orbit. On the shallow-side, the trajectories dissipate too little energy to the point of exiting the atmosphere with large positive apoapsis errors (e.g. overshooting the target). The cases presented in Figure 12 are elliptically captured trajectories. The uncaptured trajectories remain hyperbolic and are representative by too shallow entry flight path angles.

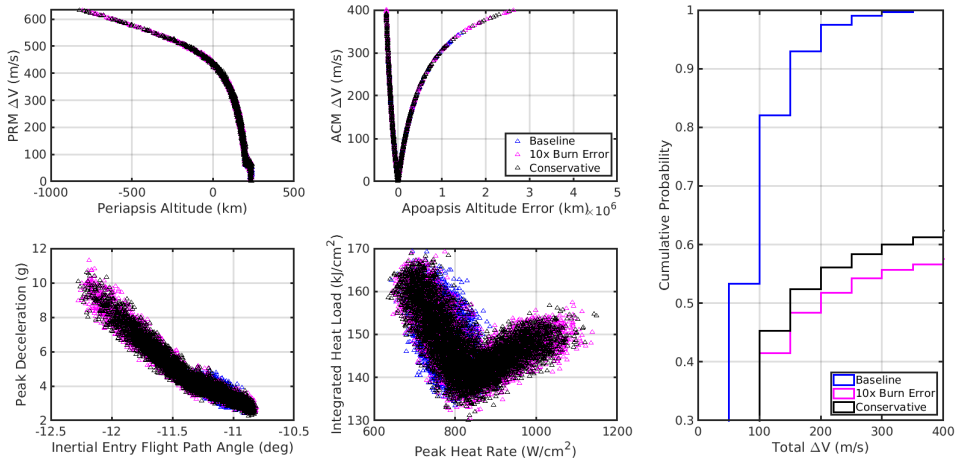

Fig. 12 Uranus Aerocapture performance for Worsened Navigation Scenarios

This results presented in this section illustrate the sensitivity of Uranus aerocapture performance and success to delivery state error. The current baseline navigation scenario provides sufficiently large enough flight path angle uncertainty to have 100% capture success. Any larger set of dispersion would lead to hyperbolic trajectories. Reductions in the dispersons would serve to buy back control margin and improve orbit insertion targeting performance.

C. Arrival Trajectory Sensitivity

This section will introduce Monte Carlo results from assessment of different arrival trajectory velocities on aerocapture performance.

Launch opportunities in the early 2030s can take advantage of a Jupiter gravity assist to reduce interplanetary transit time between Earth and Uranus. Such faster arriving trajectories have higher arrival V_∞. Designing the Jupiter flyby can allow for a wide range of possible arrival V_∞. Consequently, the sensitivity of faster arriving trajectories associated with early 2030 launch opportunities is assessed in this section. This assessment is conducted by sweeping through V_∞ values ranging from 10 to 20 km/s. Note that the baseline scenario introduced in this section has a V_∞ value of 13.6 km/s. Corridor width assessment, introduced in Section III, is used to determine the nominal entry flight path angle.

Figure 13 shows the aerocapture orbit insertion performance for the faster arrival trajectories. All 8000 simulated trajectories per arrival velocity capture into orbit. As entry velocities increase, the post-aerocapture periapsis altitude becomes smaller thereby increasing the corresponding raise maneuver cost. However, the amount of increase in minimal. The apoapsis targeting performance is generally the same between the trajectory cases but more higher ΔV cases exist the faster the entry trajectory becomes. This is evident in the total ΔV histogram where the cumulative probability per bin (width of 50 m/s) increases with decreasing arrival velocity. Nevertheless, the main sensitivity associated with faster arrival velocity is increased deceleration and aeroheating environment generally increasing non-linearly. Consequently, structural and thermal protection system capability may limit the upper-bound of arrival velocities.

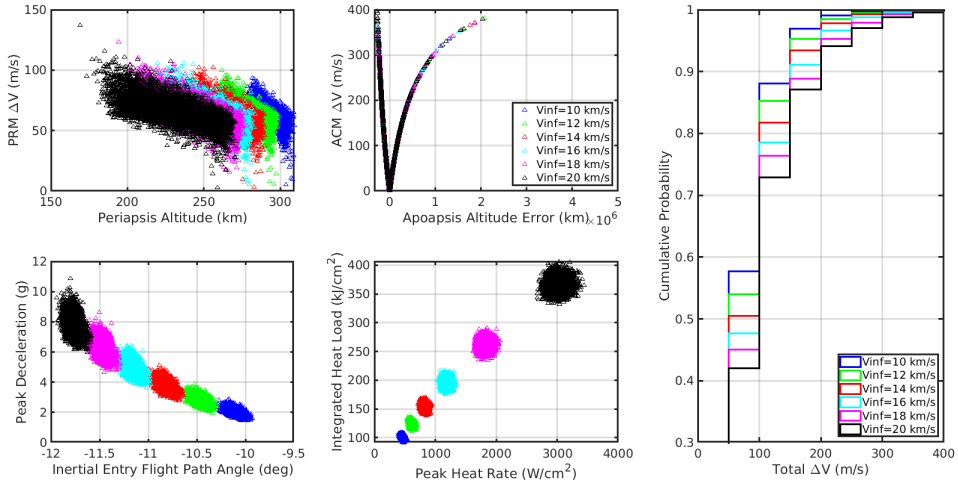

Fig. 13 Uranus Aerocapture performance for Fast Arrival Trajectories

If achieving launch opportunities in the early 2030s with Jupiter flyby is not achievable, then the resulting affect is slower arrival trajectories with lower V_∞. Corridor width trends suggest a reduction in width margin as V_∞ decreases. Consequently, an important sensitivity to understand is what implications do these slower arrival trajectories have, if any, on aerocapture performance. This assessment is conducted by sweeping through V_∞ values ranging from 5 to 10 km/s, which correspond to interplanetary trajectory solutions for launch opportunities in the late 2030s. Corridor width assessment, introduced in Section III, is used to determine the nominal entry flight path angle.

Figure 14 shows the aerocapture orbit insertion performance for slower arrival trajectories. For these lower arrival velocities, the opposite trends of the faster arrival velocities are exhibited. With respect to aerocapture performance, the apoapsis targeting performance generally remains the same while maintaining 100% capture success rate.

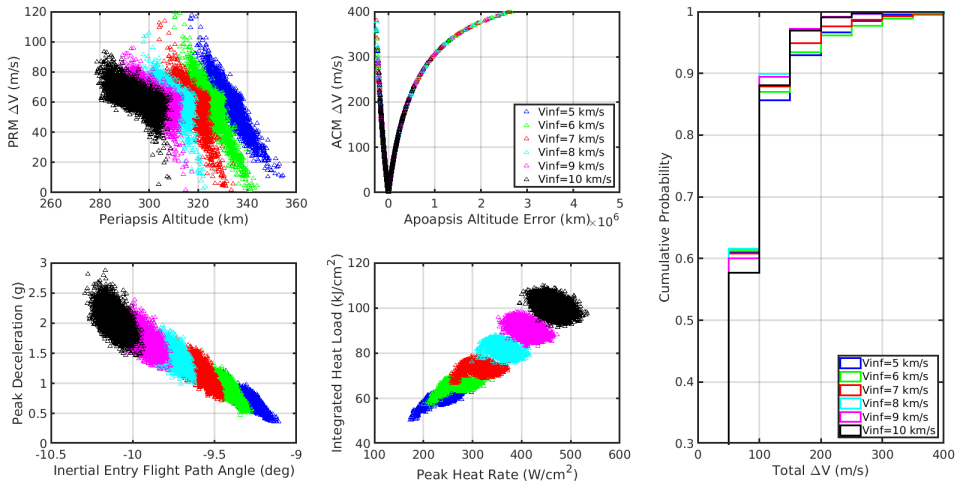

Fig. 14 Uranus Aerocapture performance for Slower Arrival Trajectories

The results presented in this section demonstrate the flexibility of aerocapture as a viable orbit insertion methodology over a wide range of interplanetary arrival trajectories.

D. Atmosphere Sensitivity

This section will introduce Monte Carlo results from assessment of different atmosphere model on aerocapture performance. Utilize atmosphere model developed by atmosphere scientists vs UranusGRAM.

One of the key risk areas associated with Uranus aerocapture is the atmosphere knowledge of Uranus. As scenario is developed where the onboard FNPAG guidance is tuned using UranusGRAM 2021 but the truth atmosphere model being simulated in POST2 comes from a tabulated custom Uranian atmosphere model, developed by atmosphere scientists (todo: get a better description of this model from Justin Garland). The idea of this sensitivity study is to assess how well the guidance can adjust to a completely different atmosphere profile than its tuned against. Figure 15 provides a visual comparison between mean, min (-3σ), and max (+3σ) density profiles between UranusGRAM and custom atmosphere model. The custom atmosphere model profiles converge to the same density profiles below 550 km but vary more than UranusGRAM above 550 km. In the region between 400 km and 550 km, the custom model has densities greater than the largest UranusGRAM profile. Between 300 km to 400 km, the custom model is bounded between the mean and +3σ UranusGRAM profiles. Below 300 km, the custom model has densities lower than the -3σ UranusGRAM profile.

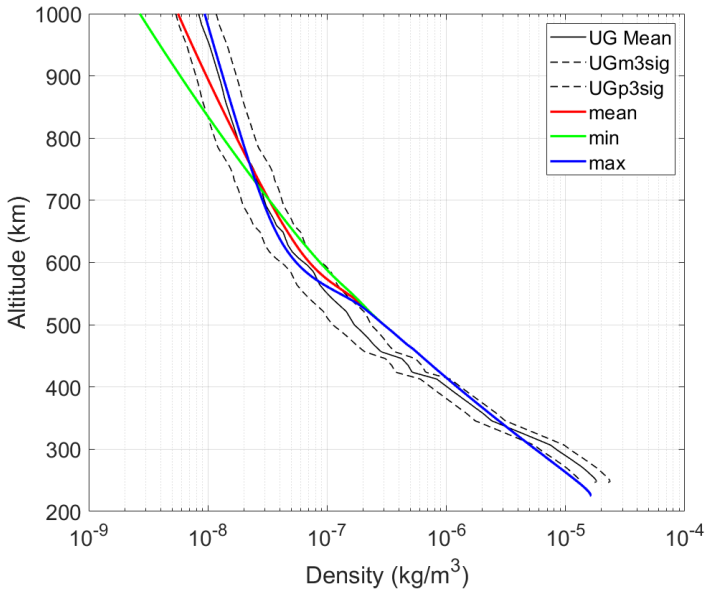

Fig. 15 Comparison of Uranus Atmosphere Profiles

Figure 16 shows the aerocapture performance comparison between the Baseline scenario and the atmosphere sensitivity scenario. The FNPAG guidance is generally able to compensate for the errors in density knowledge to the point of providing similar capture success rate as the baseline scenario. With the custom atmosphere model, the guidance tends to overshoot the apoapsis target leading to a larger correction ΔV and hence increase in total ΔV cost. The differing density profile with the custom atmosphere model leads to a reduction in the peak deceleration and peak heat rate.

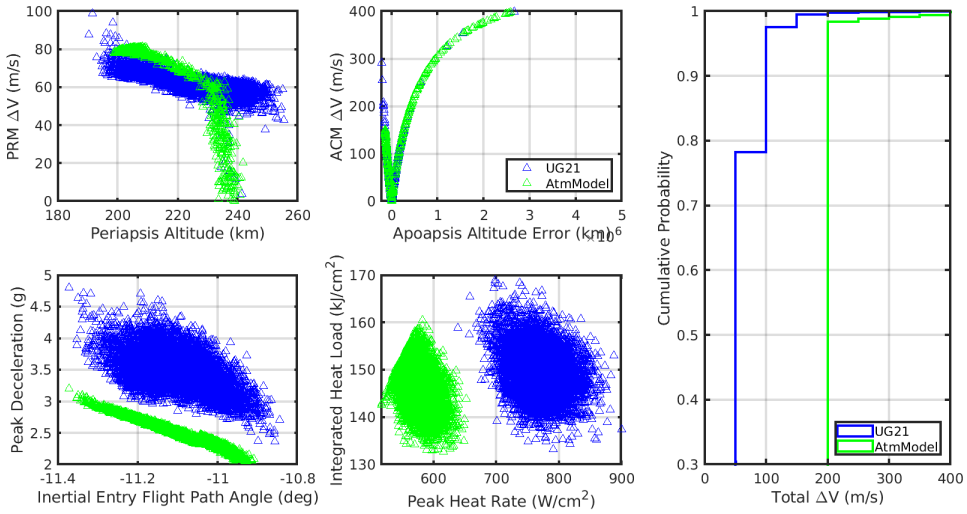

Fig. 16 Uranus Aerocapture performance for Different Atmosphere Models

VI. Conclusion and Future Work

The results presented in the paper provide a trajectory viability of an aerocapture mission for an Uranus orbiter and probe. A MSL-heritage aeroshell concept is developed and analyzed for bank angle modulated aerocapture. A 3DOF Monte Carlo sensitivity campaign was conducted to assess the robustness of the guidance to a variety of scenarios including arrival navigation, arrival trajectory, and atmosphere profiles. The performance results show good promise for the viability of Uranus aerocapture.

Future work includes further FNPAG guidance tuning to improve aerocapture performance. Trade studies on alternative flight control stratergies including direct force control and drag modulation will be investigated. Additional efforts will be put into developing and analyzing 6DOF aerocapture simulation.

References

[1] "Origins, Worlds, and Life: A Decadal Strategy for Planetary Science and Astrobiology 2023-2032," Tech. rep., The National Academies Press, 2022. https://doi.org/10.17226/26522.

[2] Rymer, A., Clyde, B., and Runyon, K., "Neptune Odyssey: Mission to the Neptune-Triton System," Tech. rep., National Aeronautics and Space Administration, 2020.

[3] Simon, A., Nimmo, F., and Anderson, R., "Uranus Orbiter and Probe: Journey to an Ice Giants System," Tech. rep., National Aeronautics and Space Administration, 2021.

[4] Hall, J., Noca, M., and Bailey, R., "Cost-Benefit Analysis of the Aerocapture Mission Set," *Journal of Spacecraft and Rockets*, Vol. 42, No. 2, 2005, pp. 309–320. https://doi.org/10.2514/1.4118.

[5] Lockwood, M., "Aerocapture Systems Analysis for a Neptune Mission," Tech. rep., NASA TM 2006-214300, 2006.

[6] Deshmukh, R., Spencer, D., and Dutta, S., "Investigation of direct force control for aerocapture at Neptune," *Acta Astronautica*, Vol. 175, 2020, pp. 375–386. https://doi.org/10.1016/j.actaastro.2020.05.047.

[7] Deshmukh, R., Spencer, D., and Dutta, S., "Flight control methodologies for Neptune aerocapture trajectories," *Acta Astronautica*, Vol. 193, 2022, pp. 255–268. https://doi.org/10.1016/j.actaastro.2022.01.004.

[8] Girija, A., "A Flagship-class Uranus Orbiter and Probe mission concept using aerocapture," *Acta Astronautica*, Vol. 202, 2022, pp. 104–118. https://doi.org/10.1016/j.actaastro.2022.10.005.

[9] Dutta, S., Shellabarger, E., Scoggins, J., Gomez-Delrio, A., R.A., L., R.G., D., Chadalavada, P., Williams, J., Garland, J., Johnson, B., Matz, D., Geiser, J., Morgan, J., Restrepo, R., and Mages, D., "Uranus Flagship-class Orbiter and Probe using Aerocapture," *AIAA SciTech,* Orlando, FL, 2024.

[10] Mages, D., Restrepo, R., R.G., D., and Benhacine, L., "Mission Design and Navigation Solutions for Uranus Aerocapture," *AIAA SciTech,* Orlando, FL, 2024.

[11] Matz, D., Johnson, B., Geiser, J., and Sandoval, S., "A Numeric Predictor-Corrector Bank-Control Guidance for Aerocapture at Uranus," *AIAA SciTech,* Orlando, FL, 2024.

[12] Shellabarger, E., Scoggins, J., Hinkle, A., Dutta, S., Deshmukh, R., Patel, M., and Agam, S., "Aerodynamic Implications of Aerocapture Systems for Uranus Orbiters," *AIAA SciTech,* Orlando, FL, 2024.

[13] Scoggins, J., A.D., H., and Shellabarger, E., "Aeroheating Environment of Aerocapture Systems for Uranus Orbiters," *AIAA SciTech,* Orlando, FL, 2024.

[14] Morgan, J., Williams, J., Venkatapathy, E., Gasch, M., Deshmukh, R., Shellabarger, E., Scoggins, J., Gomez-Delrio, A., and Dutta, S., "Thermal Protection System Design of Aerocapture Systems for Uranus Orbiters," *AIAA SciTech,* Orlando, FL, 2024.

[15] Gomez-Delro, A., and Dutta, S., "Design Implications for Aerocapture Systems Placing Flagship-class Uranus Orbiters," *AIAA SciTech,* Orlando, FL, 2024.

[16] Striepe, S., Powell, R., Desai, P., Queen, E., Way, D., Prince, J., Cianciolo, A., Davis, J., Litton, D., Maddock, R., Shidner, J., Winski, R., O'Keefe, S., Bowes, A., Aguirre, J., Garrison, C., Hoffman, J., Olds, A., Dutta, S., Zumwalt, C., White, J., Brauer, G., Marsh, S., and Engel, M., *Program To Optimize Simulated Trajectories II (POST2), Vol. II: Utilization Manual,* Version 3.0.NESC, 2015.

[17] Justh, H. L., Cianciolo, A. M., Hoffman, J., and Allen, G. A., "URanus Global Reference Atmospheric Model (Uranus-GRAM): User Guide," Tech. rep., TM 2021-0017250, 2021.

[18] Lu, P., Cerimele, C., Tigges, M., and Matz, D., "Optimal Aerocapture Guidance," *Journal of Guidance, Control, and Dynamics*, Vol. 38, No. 4, 2015, pp. 553–565. https://doi.org/10.2514/1.G000713.